Energy Conversion and Management 245 (2021) 114594

Contents lists available at ScienceDirect

Energy Conversion and Management

journal homepage: www.elsevier.com/locate/enconman

Experimental and numerical analysis of the energy performance of building windows with solar NIR-driven plasmonic photothermal effects

Enhe Zhang [a], Qiuhua Duan [a], Julian Wang [a,b,*], Yuan Zhao [a,b], Yanxiao Feng [a]

[a] Department of Architectural Engineering, Pennsylvania State University, University Park, PA 16802, USA
[b] Materials Research Institute, Pennsylvania State University, University Park, PA 16802, USA

ARTICLE INFO

Keywords:
Building windows
Solar radiation
Photothermal effect
Parametric energy simulation
Energy efficiency

ABSTRACT

Thin films made of metallic nanoparticles can exhibit strong photothermal effects (PPE) on near-infrared light irradiation, paving a way for new designs of spectrally selective building windows for solar infrared modulation that operates without the need to compensate for visible transmittance. More importantly, the surface plasmon-induced light-to-heat conversion creates strong localized heating effects with a much smaller fraction resulting in the heating of the substrate. Incorporating such nanoscale PPE into the design of complex building fenestrations, this research conducted a comprehensive analysis to better understand the PPE-induced heating effect and conductive, convective, and radiative heat exchanges between windowpane surfaces and the surrounding indoor and outdoor environments. The authors first developed and then validated a numerical analysis method to incorporate spectral features, solar spectral irradiance, and nanoscale PPE. Subsequently, using the established numerical method, two-dimensional windowpane temperature profiles and solar heat gains were yielded under different boundary conditions. To understand the energy performance of windows with solar near-infrared-dependent PPE, a series of parametric energy simulations was employed. The results show the photothermal coating can be used as a new energy-efficient retrofit technology for single-pane windows, with heating energy saving 16.2–20.8%, which performs similar to the double pane windows. Notably, these energy savings were not achieved by increasing the thermal insulation via additional layers or insulating materials, but rather by the spectrally selective design of glazing materials and utilization of solar near-infrared energy. This work presents the energy saving mechanism on an architectural scale due to the nanoscale surface plasmon-induced photothermal effect and associated heat gain coefficient enhancement. It also poses a fundamental reference for the future integration of this novel nanoscale phenomenon into the building envelope systems.

1. Introduction

Windows are essential but costly elements of building envelopes. Heat gains and losses through inefficient windows are responsible for about 30% of US building energy use, costing consumers approximately $42 billion per year [1]. Although most newly installed windows are energy-efficient double-pane or multiple-pane windows, many existing homes and commercial buildings in the US still have inefficient single-pane windows. According to the Residential Energy Consumption Survey, approximately 48.5 million single-family homes, apartment units, and mobile homes have single-pane windows, representing roughly 41% of all homes in the US [2]. As shown in Fig. 1, even in the colder Northeast and Midwest, about 27% and 26% of windows are typically single-pane windows, respectively [3]. Retrofitting single-pane glazing without changing the overall window frame and structure has long been pursued as a means of obtaining more energy-efficient performance. Practically speaking, low emissivity (Low-E) coatings are currently one of the most effective, affordable, and widely used technologies for upgrading single-pane glazing systems. In particular, Low-E windows can not only lower solar heat gain during the cooling season (since a greater fraction of the energy absorbed by such windows is prevented from entering the building), but more importantly, they also reflect long-wave infrared energy from a warm interior to reduce heat loss in the winter. Consequently, Low-E windows command a market share of 80% of residential windows and over 50% of commercial windows in the US [4]. Selecting the best type of Low-E coating for a given climate means establishing a trade-off between the ability to reject unwanted heat from the sun during cooling periods and accepting heat during heating periods. A previous study demonstrated the substantial

* Corresponding author.
E-mail address: julian.wang@psu.edu (J. Wang).

https://doi.org/10.1016/j.enconman.2021.114594
Received 23 June 2021; Accepted 29 July 2021
Available online 7 August 2021

Nomenclature

SI

Q_{abs}	Absorbed heat flow W
Q_{conv}	Convective heat flowW
Q_{rad}	Radiative heat flowW
$Q_{U-factor}$	Heat flux due to U-factorW
$Q_{solargains}$	Overall heat flux W
G_λ	Incident spectral solar irradiance W/m^2/nm
q_{abs}	Absorbed solar irradiance W/m^2
q_{trans}	Transmitted solar irradiance W/m^2
h_i	Convective heat transfer coefficient of window inner surface W/(m^2·K)
h_{con-NP}	Convective heat transfer coefficient of the NP coating surface W/(m^2·K)
$T_{NP,s}$	Temperature of the NP coating surface K
$T_{in,s}$	Temperature of window inner surface K
R_h	Interfacial insulation m^2·K/W
c	Heat capacity J/(gm·K)
ε_i	Emissivity of the inner window surface
ε_{NP}	Emissivity of the NP coating surface
τ_λ	Spectral Transmittance
α_λ	Spectral Absorptance
τ_s	Solar transmittance
α_s	Solar absorptance
N_i	Inward-flowing heat fraction
λ	Wavelength nm
A_s	Glazing surface area m^2
m	Mass g
T_o	Outdoor temperature K
$T_{glass,s}$	Temperature of soda-lime glass surface on the NP coating side K
T_∞	Ambient air temperature K
T_i	Indoor temperature K
t	time s

Abbreviation

SHGC	Solar heat gain coefficient
$SHGC_{PPE}$	Nanoscale PPE-induced solar heat gain coefficient
VT	Visible transmittance
NP	Nanopaticle
PPE	Plasmonic photothermal effect
Low-E	Low emissivity
NIR	Near-infrared
LSPR	Localized surface plasmonic resonance

challenges associated with achieving coincident high solar infrared transmittance and low thermal emissivity from longwave radiation [5]. For instance, high solar heat gain coefficient (SHGC) Low-E coatings (e.g., single silver units) can maintain a Low-E of less than 0.1, but may still reflect more than 50% of solar near-infrared (NIR) energy to the outdoor.

From the solar radiation perspective, under clear sky conditions, the irradiation energy of the NIR region occupies ~ 57.6% of global solar radiation, depending on the geographic region in the US. Even under cloudy sky conditions, the proportion is ~ 52.4%, on average [7]. This is essentially a "free" source of energy for buildings, but the radiation received is normally reflected by windows, due to the existence and unavoidable use of Low-E coatings. Therefore, the challenges reside in discovering how to achieve spectrally selective absorption of solar radiation (rather than spectrally selective reflection) and learning how to utilize this solar energy to improve the overall thermal performance of single-pane windows. However, due to the weak thermal insulation of single-pane windows, the absorbed solar NIR may be easily dissipated to the outdoor. This challenge is potentially (at least partially) alleviated through the recently discovered localized plasmonic photothermal effect (PPE) of nanostructures.

In recent years, many studies have been dedicated to exploring the surface plasmon-induced or -enhanced characteristics of plasmonic nanoparticles, which enables a wide range of applications, such as significant and tunable light absorption [8,9], light extraction in solid-state emission, photocurrent generation by harvesting below-gap photon

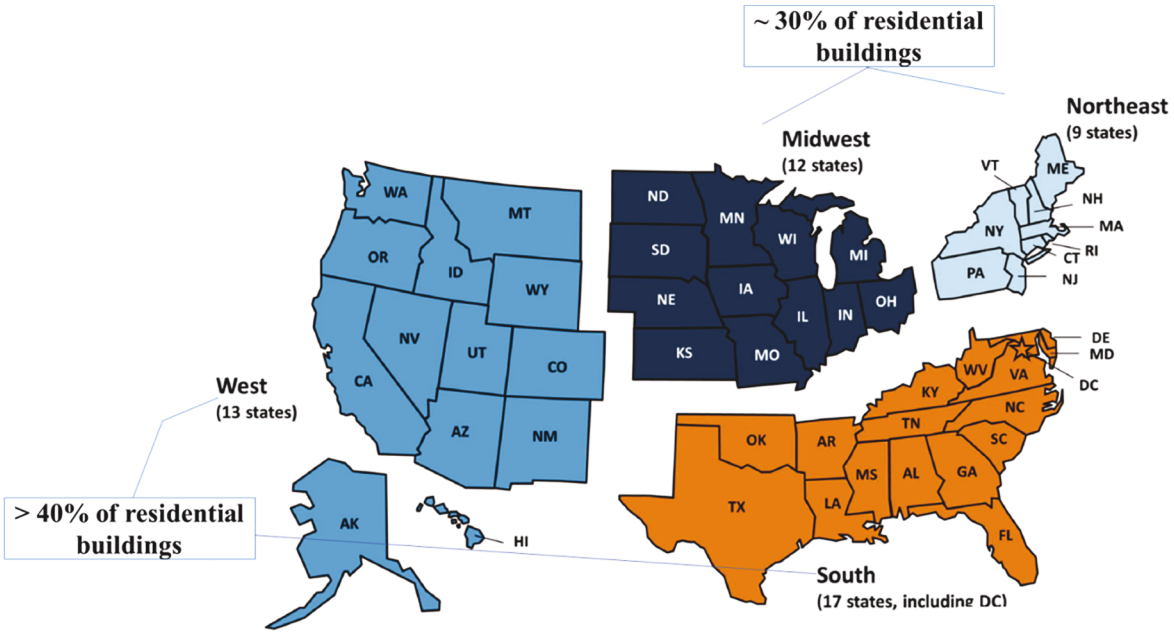

Fig. 1. Single-pane window use in the US (data adapated from study [6]).

energy in photovoltaic platforms [10,11,12], and tailored thermal emission for radiative cooling [13,14], and near-field thermophotovoltaics [15,16]. In particular, the localized surface plasmonic resonance (LSPR)-induced local heating opens new horizons in the management of thermal properties and thermal transfer characteristics. Such localized PPEs have been investigated extensively in relation to biomedical applications [17,18,19] and solar energy engineering [20]. PPE generally encompasses two stages: photonic energy absorption and photon-induced heat generation. The first stage is usually absorption but may exist in other photonic extinction states due to the microstructure of the material (e.g., multiple scatterings). The second stage is the conversion of absorbed photon energy into thermal energy. For metallic and some semiconductor NPs, LSPR is believed to be the main reason for PPE [21]. As shown in Fig. 2, driven by photoexcitation, LSPR occurs when the incident frequency matches the natural frequency of the oscillating surface electrons. This excitation causes inhomogeneity in the electron density of the conductor, generating a local electrical field that tends to drive charge equilibration. Electrons accelerating through this field can acquire enough energy to overshoot the equilibrium configuration and effectively switch the local electric field, causing oscillation.

More importantly, recent experiments have demonstrated that the LSPR-induced localized heating of plasmonic NPs may become quasi-ballistic (when the particle size is much smaller than the phonon mean free path in the substrate [22]) which could result in nonequilibrium of phonon transport from the localized surface hot spots and also introduce significant thermal barriers [23], or great thermal conductivity reduction of surrounding medium or substrate [24,25,26]. This LSPR-induced localized heating feature has been used for creating superheated surfaces [27,28] and even localized phase transition [29,30] while still keeping the medium or substrates still close to ambient temperature. Although the fundamental mechanism to understand such complex photo-thermal processes is still being explored, some experiment-based studies have consistently noted that the conventional heat transfer model failed to characterize the temperature increase in these plasmonic nanoscale systems [23,24,31]. It has been found that the plasmon-induced temperature rise is significantly higher than the computed one upon the conventional heat transfer model [23], and also much greater than the same materials but without plasmonic NPs under the same irradiation [24]. **From the window application perspective, these strong surface-localized heating can be extremely useful due to their directional or tailored thermal emission, which could potentially enhance the inward-flowing heat fraction.**

Furthermore, several types of metallic NP show strong extinction peaks in the NIR region of the electromagnetic spectrum and exhibit a strong PPE. Photonic extinction comes in two forms: scattering and absorption. According to the Mie scattering theory, absorption and scattering are heavily dependent on particle size. Particles with sufficiently small diameters (e.g., 10% of the incident wavelength) interact with light primarily by absorption rather than scattering. The wavelengths at which NPs interact with light, as well as their ratio of absorption and scattering abilities, can be tuned by varying their composition, shape, and size[18]. Such NPs are capable of modulating light on a nanoscale and can be incorporated into glazing systems with spectral selectivity in the solar NIR region. Li et al. [32] synthesized antimony-doped tin oxide (ATO) to create a spectrally selective thin film that efficiently reduced NIR transparency. Less solar heat was transmitted upon NIR absorption. The authors reported 1.5 °C to 4.5 °C lower temperatures under a 100 W infrared lamp at room temperature (than with commercial glass), indicating a potential use in building windows for cooling purposes in the summer season. Besteiro et al. [33] described an approach for designing passive solar NIR-blocking glass using plasmonic nanocrystals made of noble (Ag and Au) and alternative materials (TiN, Al, and Cu). The resulting coating was capable of blocking solar NIR, starting with wavelengths of 700 nm to 1,700 nm, due to the absorption caused by the plasmonic resonance. This design focused on building window applications for cooling in the summer season. Yet, the SHGC analysis ignored the heat flowing inward because of NIR absorption. Shen et al. [34] synthesized Sb-doped SnO_2 (ATO) powder via a dual-titration coprecipitation method and tested its optical performance specifically in the region from 1,500 nm to 2,500 nm. The authors demonstrated a 76% NIR blocking ability attributable to its localized surface plasmon resonance (LSPR), emphasizing the potential use of such methods in building windows for cooling purposes. They also noted that although the NIR energy was absorbed, most of the heat was believed to return to the outdoor environment. But no specific heat transfer analysis was conducted to demonstrate that belief. Zhao et al. [35] examined the PPE of PAA-Fe_3O_4 nanoparticle solutions stimulated by a 1,000 W/m^2 785 nm laser. The researchers found that the temperature in the indoor environment increased 3.5 °C within 15 min. They also tested the influence of NP size on the peak wavelength of infrared light absorption. Based on simple U-factor calculations for the temperature increase data, the authors predicted a potential heating energy savings of 85 to 159 KJ/m^2 in 1 h of white light irradiation. Guo et al. [36] designed transparent solar thermal surfaces with Au NP assemblies. The in-plane linear Au NP assemblies exhibited longitudinal plasmon absorption under solar NIR and caused a strong PPE with more than 65% visible transmittance (VT). Under 1 h of sun exposure, the temperature of the solar thermal surface with Au NP assemblies increased up to 9.8 °C in room temperature situations, thus reducing heating energy use. Lyu et al. [37] investigated the PPE of thin chlorophyll and chlorophyllin films, finding peak absorption near the UV and NIR regions. They also identified a light angle dependence of the absorption and photothermal heating effects. Maximum temperature increases were achieved at a 20° incident angle. This nanostructured window design was also designed for heating energy savings in winter.

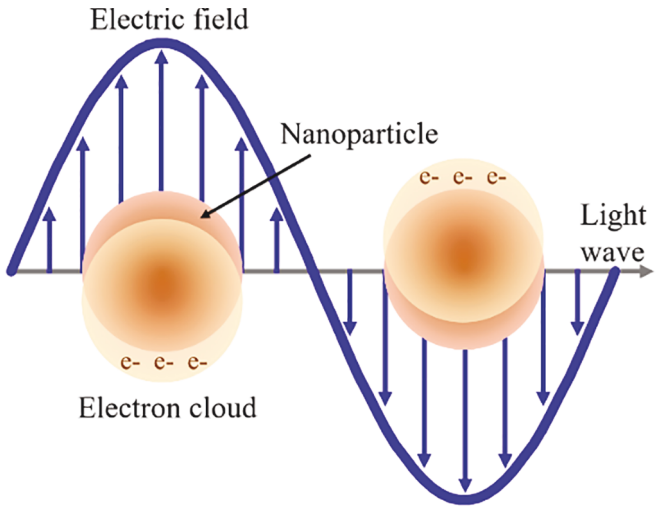

Fig. 2. Schematic diagram of LSPR.

As discussed above, although a few studies have claimed that nanoscale PPE can potentially be used in building window-related applications, much less attention has been paid to comprehensively analyzing the thermal and optical behaviors of the nanoscale PPE employed in glazing, let alone its overall energy performance. Therefore, the above-mentioned studies have led to conflicting conclusions. Some studies have focused on plasmonic NPs' NIR absorption and suggested their use in blocking solar heat for cooling purposes [32,33,34], while others addressed the NIR absorption induced by LSPR, concluding that it offered the potential of heat-related energy savings in winter [35,36,37]. The controversy is because the energy performance of building windows depends on both their thermal and optical features, such as surface emittance, thermal conductivity, spectral absorptance, and spectral transmittance. Briefly, the strong absorption of solar NIR may block the solar transmittance and reduce the overall solar heat gains, but the enhanced inward-flowing heat due to the nanoscale LSPR-

induced PPE may offset and even outweigh the reduced solar heat gains. Therefore, before incorporating nanoscale PPE into glazing systems, a comprehensive heat transfer and energy performance analysis at the building scale must be conducted.

In the present research, an analytical model for characterizing the thermal performance of single-pane windows incorporated with nanoscale PPE is proposed, validated, and then utilized in a parametric building energy analysis. It is important to note that this model development is not to solve the above issue related to the quasi-ballistic heat transfer away from or between the plasmonic NPs and/or surfaces on the nano-structural scale. Rather, this model focuses on the architectural scale and is built upon the experimental data obtained from photothermal testing of single-pane glass coated with selected plasmonic NPs.

The contribution of this paper is threefold: **First**, the nanoscale surface plasmon-induced PPE has been found with very unique surface localized heating features, for which the conventional heat transfer model is unable to characterize. To do so, a new analytical model was established to take the nanoscale PPE and its quasi-ballistic heat transfer mode into account. The simple estimate is based on rudimentary approximations, but it most importantly shows the directional heat dissipation of single-pane windows is energetically possible. With this model, exact solutions for two-dimensional temperature profiles and overall solar heat gains can be established. Moreover, the model established in this work can be expanded into double-pane window systems or other multiple glazing structures consisting of one windowpane coated with photothermal NPs. **Second**, the effect of the surface plasmon-enhanced temperature rise on inward heat flow is demonstrated, and associated with solar heat gain coefficients of single-pane windows under various boundary conditions are analyzed. This elucidates the energy-saving mechanism of applying such nanoscale PPE effects for single-pane window design. Also, a dynamic SHGC concept has to be engaged in the energy performance analysis of the photothermal windows due to the strong solar absorptance and unique inward-flowing thermal behaviors of photothermal windows. **Third**, to the best of our knowledge, this is the first work to incorporate nanoscale surface plasmon-induced PPE into comprehensive energy analysis at the building scale. The energy savings relative to the typical Low-E coated single-pane windows and double-pane windows were quantified, and the energy-saving potentials of the photothermal windows across different climates were provided. Meanwhile, the parametric energy simulation method used to simulate photothermal windows in this work can be also useful to energy estimation of other smart glazing systems with dynamic SHGC.

The paper is organized as follows. Section 2 describes the analytical model development and experimental validation. In Section 3, the analytical model is used to derive a relationship between the solar heat gains by the nanoscale PPE and the boundary conditions. In Section 4, a comprehensive whole-building energy analysis is presented, and the energy performance of the photothermal windows is compared with both single-pane and double-pane windows. Finally, Section 5 gathers the conclusions of this study.

2. Analytical model development and experimental validation

2.1. Theoretical analysis

The overall heat transfer occurring under solar radiation is shown in Fig. 3. For building windows, solar radiation is transmitted, absorbed, and reflected in varying amounts, depending on the window's optical properties and ambient environmental conditions. Transmitted solar radiation can directly reduce space heating needs. In contrast, absorbed solar radiation may partially flow inward from the panes to the indoors, possibly increasing the indoor temperature and consequently improving heating energy savings in winter. The fractions of these elements are referenced by the solar heat gain coefficient (SHGC) parameter in the fenestration area. The absorbed solar irradiance (q_{abs}) was calculated by Equation (1). Similarly, the solar irradiance (q_{trans}) transmitted by the glazing system was obtained by Equation (2). Solar irradiance can increase the glazing system's temperature, especially in photothermal windows.

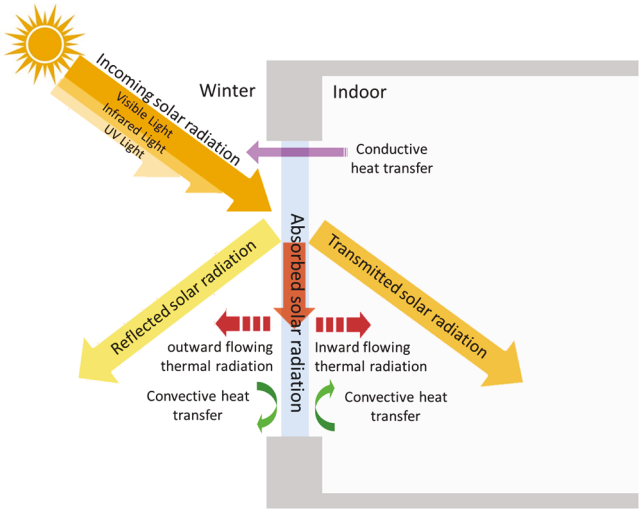

Fig. 3. Solar radiation and window thermal transfer.

$$q_{abs} = \int G_\lambda \alpha_\lambda d\lambda \tag{1}$$

$$q_{trans} = \int G_\lambda \tau_\lambda d\lambda \tag{2}$$

where G_λ is the incident spectral irradiance from solar light or simulated solar light and α_λ is the spectral absorptance of the photothermal coated windows.

The solar energy absorbed by a glazing system can be obtained with the given glazing area, which may spontaneously increase the glazing system's temperature. In conventional steady-state heat transfer model, this thermal energy-driven temperature change can be expressed by:

$$\frac{dT}{dt} = \frac{1}{c*m}*\left(\sum Q_{in} - \sum Q_{out}\right) \tag{3}$$

$$Q_{in} = q_{abs}{}^{*}A_s \tag{4}$$

$$Q_{out} = Q_{conv} + Q_{cond} + Q_{rad} \tag{5}$$

where the heat capacity (c) is in units of J/gm K, m is the material mass in gm. Under the designed internal and external boundary conditions, Q_{in} is obtained from the absorbed solar irradiation on window surface (Eq. (4)), Q_{out} is including all conductive, convective, and radiative heat transfer from both interior and exterior surfaces of the overall glazing system (Eq. (5)). This was more complicated, considering the convection flow and emissivity features of the glazing system surfaces. Under uniform and constant indoor and outdoor air conditions and stable continuous solar irradiance, the energy balance model could be developed to perform energy balance analyses and identify temperature characteristics. In the conventional calculations, the glazing system is deemed as a homogenous bulk, so the temperature rise calculated from Eq. (3) equally occurs on two surfaces.

However, as discussed in the introduction section, when the plasmonic NPs are coated on the surface of the glazing material, the LSPR-induced PPE may significantly enhance the temperature rise of the coating surface with a smaller fraction of heat flow to the substrate. This could be explained by the great heat transfer reduction between the NPs and the substrate driven by the quasi-ballistic effect because the particle size is much smaller than the phonon mean free path in the substrate material[26]. Inspired by the prior study about LSPR-induced solar

vapor generation[23], a hypothesized interfacial insulation (R_h) between the nanoscale plasmonic NPs coating and the glazing was incorporated and substrated into the conventional heat transfer model. In the stable boundary situations and same ambient temperature conditions, the absorbed solar energy Q_{in} equals the sum of the heat dissipated from the NP-coated surface and the conductive heat transfer away from the NP-coated layer to the glass through the interfacial layer. The mathematical expression of Q_{out} is provided below.

$$Q_{out} = h_{con-NP}\left(T_{NP,s} - T_{\infty}\right)A_s + \varepsilon_{NP}\sigma\left({T_{NP,s}}^4 - {T_{\infty}}^4\right)A_s + \left(\frac{1}{R_h}\right)\left(T_{NP,s} - T_{glass,s}\right)A_s \quad (6)$$

where $T_{NP,s}$ is the surface temperature of the coating layer, $T_{glass,s}$ is the soda-lime glass surface temperature on the coating side. So, ($T_{NP,s}$ - $T_{glass,s}$) represents the temperature difference between the two sides of the hypothesized interfacial insulation. T_{∞} is the ambient air temperature. The interfacial insulation R_h is determined by fitting the analytical surface temperature model to the measured surface temperature data. $h_{con\text{-}NP}$,ε_{NP}, σ are parameters involved in the heat transfer of the photothermal coating surface. Notably, this function is different from the conventional macroscopic heat transfer model in which conductive heat transfer directly happens from the photothermal coating layer to the soda-lime glass substrate. In other words, the presence of interfacial insulation is assumed to create heat flow barriers and then match the enhanced heat dissipation from the coating surface. Then, by combing Eqs. (3)–(6), the 2D temperature profiles from the initial status under irradiation to the stead-state can be solved analytically.

2.2. Experiments for model validation

To apply the model in practice, photothermal experiments under a solar simulator in the lab were conducted, as shown in Fig. 4**a**. The specific metallic NPs selected was Fe_3O_4@$Cu_{2-x}S$, which have been found to have robust spectrally selective absorption of NIR radiation with only a minor reduction in the visible region. The material exhibits highly efficient photothermal heating conversion under continuous illumination at room temperature. The synthesis and basic characterizations of the photothermal NPs, Fe_3O_4@$Cu_{2-x}S$, can be found in previously published work [38]. A previous study by Tian et al. described nanoparticle size-dependent Fe_3O_4@$Cu_{2-x}S$ NPs, in which the absorption peak shifted from 960 to 1,150 nm as the particle size increased from sub-10 to 15 nm [39]. Therefore, average-15 nm-sized Fe_3O_4@$Cu_{2-x}S$ NPs were prepared and used. The Fe_3O_4@$Cu_{2-x}S$ NP solutions were spin-coated on glass panes (~2.5 * 2.5 cm^2) for 10 s at 1,000 rpm at different concentration levels. In particular, the mass of NPs thin-film per coating area on the glass is 2.54 × 10^{-4} g/cm^2. Then, the spectral characteristics (i.e., spectral transmissivity and reflectivity) of the coated glass were measured using a LAMBDA 900 UV/Vis/NIR spectrophotometer (See Fig. 4**b**). The sample was irradiated with 1,000 W/m^2 irradiance by a Newport 150 W solar simulator. The temperature was continuously monitored by a FLIR E6 infrared camera.

The experiments show that the surface teperatures on the Fe_3O_4@$Cu_{2-x}S$ NPs coating side increased very rapidly under the simulated solar light radiation, reaching a temperature plateau within 10 min. The solar simulator was turned off at the 10th minute and the sample's temperature was continuously recorded during the cooling-down period.

To ensure the validation, in the analytical model calculation procedure, we input same ambient conditions and material properties that were used in the experiments. The key variables are shown in Table 1. In the conventional approach, the temperature of this coating surface can be calculated using the heat transfer equation and these key variables of the experiment. Fig. 5 depicts the measured and calculated (via the conventional method) temperature rise of the glass coating surface. The drastic disagreement echoes the finding in other surface-plasmon-induced local heating studies that the conventional heat transfer model is not able to estimate nanoscale PPE [23,24,31].

As mentioned above, the presence of the interfacial insulation was assumed to match the enhanced temperature rise by the PPE. By fitting the analytically calculated surface temperature to the measured data above, $R_h = 0.03$ m^2K/W was obtained. In other words, a thermal barrier appears when it comes to the surface plasmonic resonance of the Fe_3O_4@$Cu_{2-x}S$ NPs and reduced the effective thermal conductance to another side of the glazing.

To validate the analytical model with the fitted interfacial insulation,

Table 1
Key Variables in Experiments and used for the Analytical Model.

Illumination power	1,000 W/m^2
Glass plate	0.0254 * 0.0254 m^2
Thermal conductivity of glass	0.8 W/(m·K)
Coating mass	1.6 * 10^{-3} gm
Coating emissivity	0.06
Glass emissivity	0.84
Ambient air temperature	298 K
Indoor relative humidity	30%

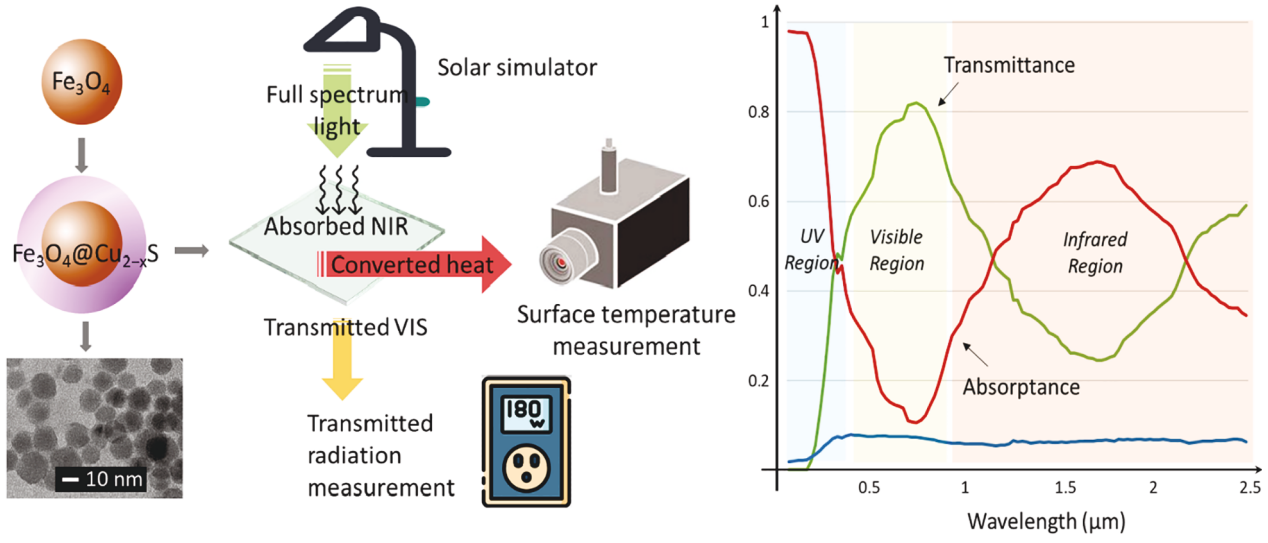

Fig. 4. a) Diagram of the photothermal experiment. b) Spectral characteristics of Fe_3O_4@$Cu_{2-x}S$ NPs coated glass pane.

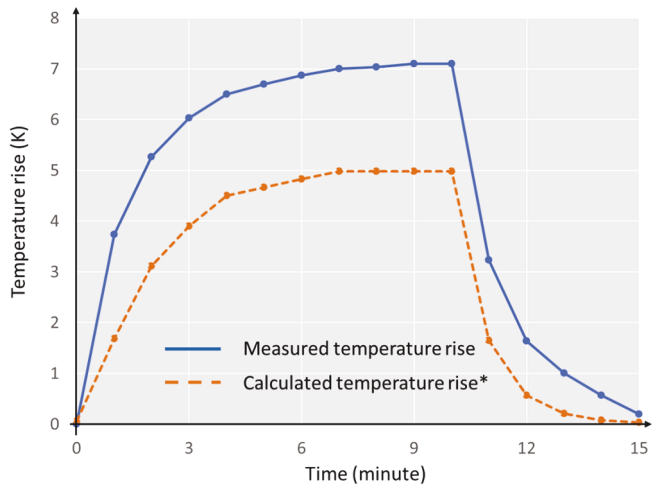

Fig. 5. Measured temperature rise of $Fe_3O_4@Cu_{2-x}S$ NPs coated glass and calculated temperature rise (*via the conventional heat transfer equation).

the comparison was made for the calculated temperature profiles of $Fe_3O_4@Cu_{2-x}S$ NPs coated glass samples with the different irradiation levels (absorbed light irradiation ranged from 50.8 to 155.9 W/m^2). The experimental data in this validation procedure were adapted from the study [29]. The validation results are shown in Fig. 6 and consist of two sets of temperature rise generated from the experiments and simulated via the established model. This shows the proposed analytical model is in good agreement (~0.09 mean relative error and 0.95 R square) with the experimental data with respect to the temperature rise.

3. Implementation for energy analysis of LSPR-induced photothermal windows

The validated model that includes nanoscale PPE helps to resolve the question of whether photothermal windows can be considered a means of saving building heating energy for single-pane windows in winter. This section describes the implementation of the analytical model into a whole building energy performance analysis. First, two window models were built – single-pane Low-E and single-pane photothermal windows, using the LBNL WINDOW software that implements ISO 15099 window calculation standard [40], and is also certified by the National Fenestration Rating Council (NFRC) [41]. The Low-E coating selected was a single layer and silver-based (emissivity 0.05) and placed on the inner surface. Because of the main focus on heating energy savings in this work, this selected Low-E coating had a relatively higher solar transmittance (τ_s) and suitable for heating-dominated climates. The spectral data of $Fe_3O_4@Cu_{2-x}S$ NPs coated glass measured in the lab were imported manually into the program according to the data compliance requirements. Subsequently, this program was used to output the thermal and optical properties.

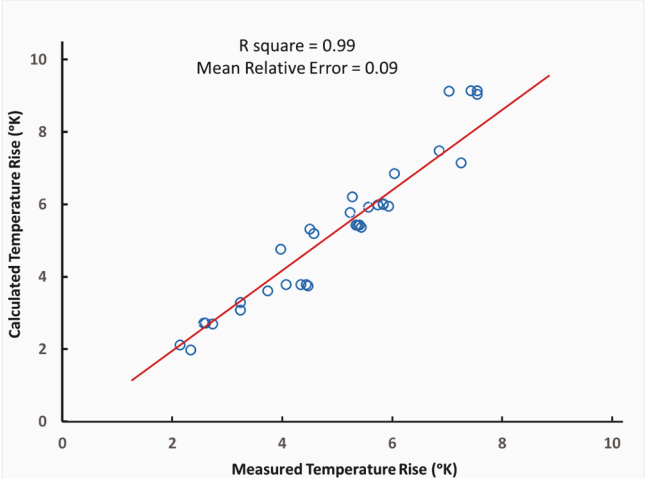

Fig. 6. Validation of experimental data and calculated data by the analytical model with R_h.

The detailed spectral characteristics for the photothermal window are provided in Table 2. It shows that the photothermal window had a 45% absorptance (α), which is much higher than the Low-E window, while the VT of the photothermal window was only 1% lower than that of the Low-E window. More importantly, in the solar NIR band, the average absorptance of the photothermal window was about 69%, which was significantly higher than the absorptance of the Low-E window (17%). This was mainly caused by the strong NIR absorption ability of the photothermal film consisting of the $Fe_3O_4@Cu_{2-x}S$ NPs. From the reflectance perspective, within the NIR band, the Low-E window reflected about 57% of the solar NIR irradiance, while the photothermal window reflected only 6%. This significant difference between the two window models was in response to the solar infrared absorbed by the photothermal window and reflected by the Low-E window. This is a key energy savings rationale for using photothermal nanostructures in this research work. Another critical parameter was τ_s; both window models transmitted about a half of incident solar radiation, demonstrating the practical appropriateness of the designed glazing in heating-dominated climates. The Low-E and photothermal windows had very similar U-factor levels, which was related to the thermal resistance of each layer of the window structure and emissivity values. This can be explained by the fact that the thin layer of coating did not have much influence on the thermal resistance.

3.1. Solar heat gain analysis

In the conventional photo-thermal process, the higher the absorbed solar energy, the greater the temperature rise of building glazing systems. However, the inward-flowing fraction of the thermal energy converted from the absorbed solar energy may be offset by the low emissivity of the inner surface. In the NFRC SHGC calculation standard, the SHGC can be expressed as follows:

$$SHGC = \tau_s + N_i \alpha_s \quad (7)$$

where τ_s is the solar transmittance of window systems, α_s is the solar absorptance, and N_i is the inward-flowing fraction of absorbed radiation.

N_i is dependent on the overall surface heat transfer coefficients on the inner and outer surfaces of the glazing. When the solar absorptance is low, the inward-flowing heat fraction is much low, especially when the low emissivity of the inner surface presents. Meanwhile, the boundary conditions have no or slight effects on the resultant SHGC value. However, when high solar absorptance is involved, boundary conditions may have a pronounced effect on N_i. Similar issues have been found in the study [42]. Furthermore, the temperature rise in this work is not only dependent on the increased photon absorption but also the strong LSPR-induced plasmonic heating effect[24]. The LSPR-induced

Table 2
Spectral Characteristics Retrieved from LBNL WINDOW program with measured optical data of photothermal coatings.

Glazing properties	Photothermal	Low-E
Visible transmittance VT, 380–780 nm	0.75	0.76
Solar transmittance τ_s, 300–2,500 nm	0.50	0.51
Solar absorptance, 300–2,500 nm	0.45	0.16
Solar front reflectance, 300–2,500 nm	0.05	0.33
NIR transmittance, 780–2,500 nm	0.37	0.26
NIR absorptance, 780–2,500 nm	**0.57**	0.09
NIR front reflectance, 780–2,500 nm	0.06	**0.65**

PPE is governed by the electric field intensity that is formed by the collective oscillation of the energetic electrons upon resonant excitation [43]. There is an increase in the number of energetic electrons of plasmonic NPs at higher irradiation intensities, which in turn leads to a more pronounced PPE[44,45].

The analytical model validated in Section 2 enabled us to explore the relationship between the solar irradiance levels and the PPE effects on the inward-flowing fraction of the absorbed solar radiation in different outdoor air temperature conditions. A range of solar radiation values from 100 W/m^2 to 1,000 W/m^2 was selected to represent the incident solar irradiance levels at the vertical window surface. The outdoor temperature was ranging from 258 K to 313 K with a 5-degree interval. The indoor temperature was kept at 297 K. As such, 130 boundary combinations of outdoor temperature and solar irradiance were calculated. By using the analytical model, the window temperature profiles were derived across each surface, and then the inward-flowing thermal radiation, the inward-flowing fraction, and SHGC were computed. The inward-flowing fraction and SHGC calculation was based on the solar calorimetric method of NFRC 201[46], which is determined by the following Eqs. (8) and (9). To simplify the analysis, other effects resulting from incident solar angles, window frames, glazing edges, and condensation were not considered.

$$Q_{solar\ gains} = h_i A_s \left(T_{in,s} - T_i\right) + \varepsilon_i \sigma A_s \left(T_{in,\ s}^4 - T_i^4\right) \tag{8}$$

$$SHGC = \left(Q_{solargains} - Q_{U-factor}\right) \Big/ \int A_s G_\lambda d\lambda \tag{9}$$

where $Q_{solargains}$ is the overall heat flux flowing through the window under solar irradiation and given temperature boundaries, $T_{in,s}$ is the inner surface temperature of the window, T_i represents the indoor air temperature, and T_∞ is the ambient air temperature. h_i,ε_i,k_{in}, σ are

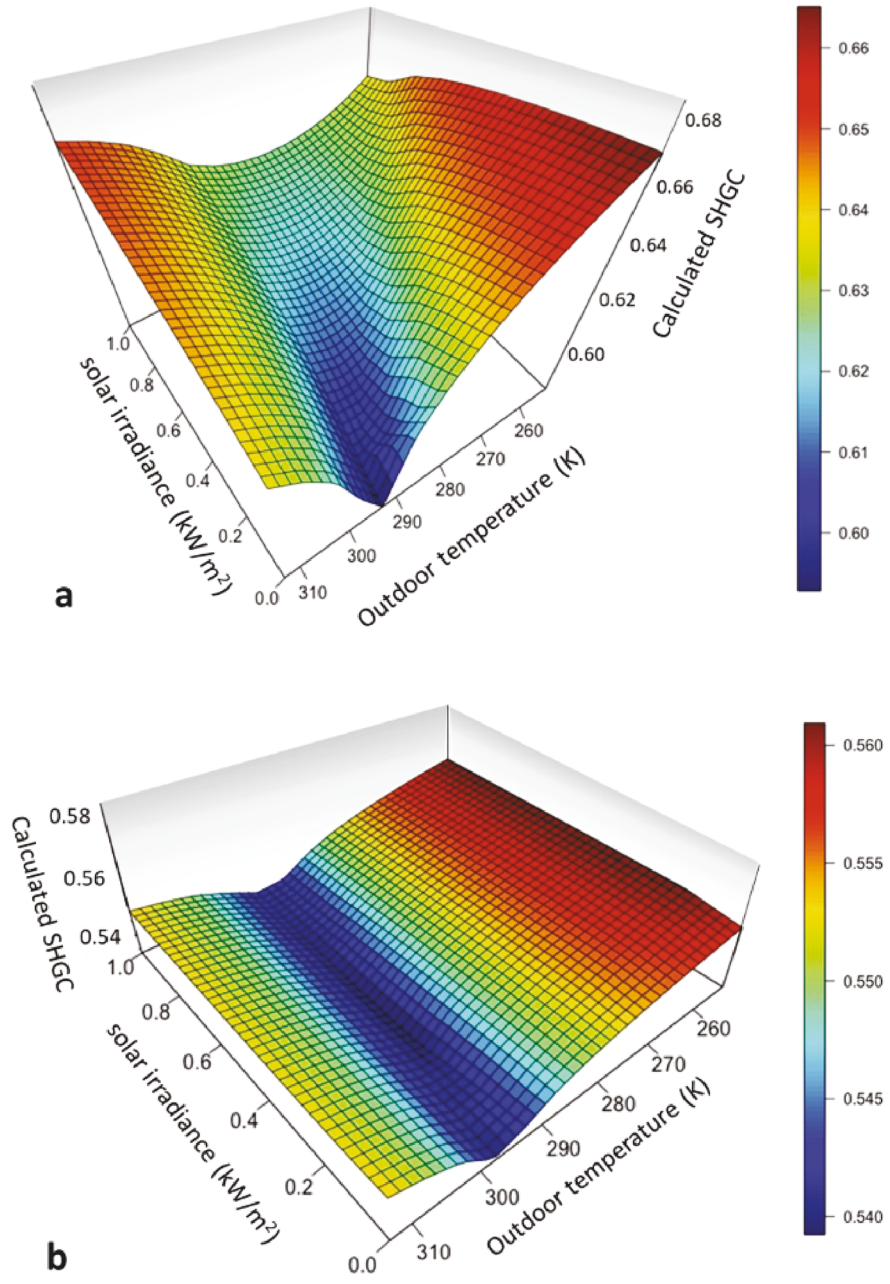

Fig. 7. SHGC data distribution of the photothermal window (a) and the Low-E window (b).

parameters or constants involved in the convective and radiative heat transfer.$Q_{U-factor}$ is the heat flux due to indoor and outdoor air temperature difference and calculated upon the overall U-factor of the window system. G_λ is the spectral solar irradiance incident on the window.

To demonstrate the differences of the photothermal windows, we also calculated the solar heat gain performance of the Low-E window model. In general, the photothermal window gained more solar irradiance than did the related Low-E window. Affected by the PPE, that difference in solar absorption resulted in a much higher different temperature increase for the inner window surfaces of the two types of windows. For instance, at 200 W/m^2 solar irradiance and 273 K outdoor temperature conditions, the Low-E window reached 280.09 K, while the photothermal window reached 286.44 K. When the incident solar irradiance was over 200 W/m^2, the window even became a thermal radiation source for the interior in certain situations. Fig. 7 shows 3D SHGC variations with different outdoor conditions for the photothermal window (a) and the Low-E window (b). It clearly shows that the SHGC values of the photothermal window range from 0.58 to 0.67 varying with outdoor temperature and incident solar irradiance, while for the Low-E windows, the solar irradiance level and outdoor temperature alter the inward-flowing fraction and SHGC values little. It is basically aligned with the output under standardized boundary conditions, which were simulated by using LBNL WINDOW. This also reveals that the standardized SHGC calculation procedure (Eq. (7)) may not have reflected actual solar heat gain variations of the photothermal window due to its strong solar NIR absorption and the presence of the interfacial insulation due to the nanoscale PPE.

The SHGC variations of the photothermal window are more complicated. It can be seen that the data points are distributed along a parabolic-like surface, and the minimum values for each incident solar irradiance level appear at specific outdoor temperatures. This feature can be also clearly seen in Fig. 8. As the solar transmittance was the same for all conditions, the SHGC variations relied on the changes of inward-flowing heat fractions. Theoretically, when the inner side temperature difference between the inner surface temperature and indoor air is minimal, little inward-flowing heat fraction is formed, thus the lowest SHGC value is yielded. For instance, at 100 W/m^2 incident solar irradiance, the inner window surface temperature reached 297.6 K when the outdoor temperature was around 293 K. Consequently, the lowest SHGC value 0.58 was yielded. Conversely, when the temperature rise by the 100 W/m^2 solar irradiation made the outer window surface reach the temperature close to the outdoor condition, the maximum SHGC 0.67 was formed. Additionally, since the variation of SHGC relies on the inward-flowing heat and is independent of solar transmittance, there is no change in the visible transmittance of the photothermal windows.

To incorporate this dynamic SHGC into the energy simulation platform for analyzing the photothermal window, a simplified mathematical model would be required. Based on the data distributions and physical meanings of SHGC, the parabolic function $y = a(x\text{-}b)^2 + c$ was used to build a mathematical model of SHGC for the photothermal window. The parameter b indicates the outdoor temperature at which y equals c, referring to the minimum SHGC. As shown in Fig. 9, the outdoor temperature (parameter b, the red curve) associated with the minimum SHGC at each level of solar irradiance is negatively correlated to solar irradiance. The parameter c (the blue curve), on the other hand, has a positive relationship to solar irradiance. The final regression model is expressed in the following Equation (10). To differentiate from the standard SHGC concept, here we used $SHGC_{PPE}$, indicating the nanoscale PPE-induced solar heat gain features.

$$SHGC_{PPE} = a(T_o - b)^2 + c \tag{10}$$

$$a = 4.5 \times 10^{-5}$$

$$b = -0.02 \times \int G_\lambda d\lambda + 297.17$$

$$c = 4.13 \times 10^{-5} \times \int G_\lambda d\lambda + 0.58$$

where $\int G_\lambda d\lambda$is the total incident solar irradiance and $T_o$is the outdoor temperature. This model can be simply interpreted from the physical perspective and also estimate the photothermal window SHGC with high accuracy (mean absolute percentage error 1.7%, root mean square error 0.01).

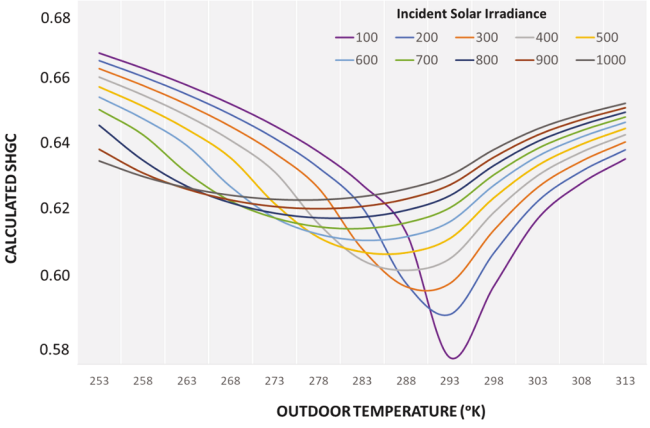

Fig. 8. Photothermal window SHGC variations with different outdoor temperatures and incident solar irradiance.

3.2. Parametric energy simulation method for incorporating $SHGC_{PPE}$

To compute the whole building energy performance while considering the dynamic features of $SHGC_{PPE}$, a parametric energy simulation method was needed that simulated the dynamic properties of building windows. The Energy Management System (EMS) module in EnergyPlus has been demonstrated suitable and effective to simulate dynamic characteristics of building envelopes in prior studies [47,48]. Compared with other parametric simulation methods, EMS may offer more rigous logics between the envelope physical parameters and the external or internal stimuli with higher resolution. This research followed these previous dynamic envelope simulation method and incorporated the dynamic $SHGC_{PPE}$ parameter into the whole building energy simulation and analysis. In this module, a simplified programming language, EnergyPlus runtime language (erl), was used to write parametric relationships and simulation logic. The EMS consists of sensors, actuators, built-in variables, and global variables. Sensors retrieve existing information in the model, while actuators are components that change in response to conditional statements. Available sensors and actuators are based on the model and provided in the RDD and EDD output files, respectively.

In this specific simulation, "Zone Outdoor Air Dry Bulb Temperature" and "Surface Outside Face Incident Solar Radiation Rate per Area" were used as the sensor parameters. The actuator related to the window type, called "Construction State," was also adopted. The calling points in this work selected "Begin Timestep Before Predictor," which occurred near the beginning of each timestep but before the zone loads were calculated. The $SHGC_{PPE}$ model (Eq. (10)) was employed to determine the SHGC values of each construction state of the building windows. The EMS parametric energy simulation workflow used in this work is provided in Fig. 10.

The DOE prototypical small office building model (1 story, ~510 m^2 floor area) and the most recent ASHRAE 90.1 standards were used as the case study. The window-to-wall ratio of this model was approximately 24.4% for South and 19.8% for the other three orientations. The only control element in the prototypical model was the windows. To better

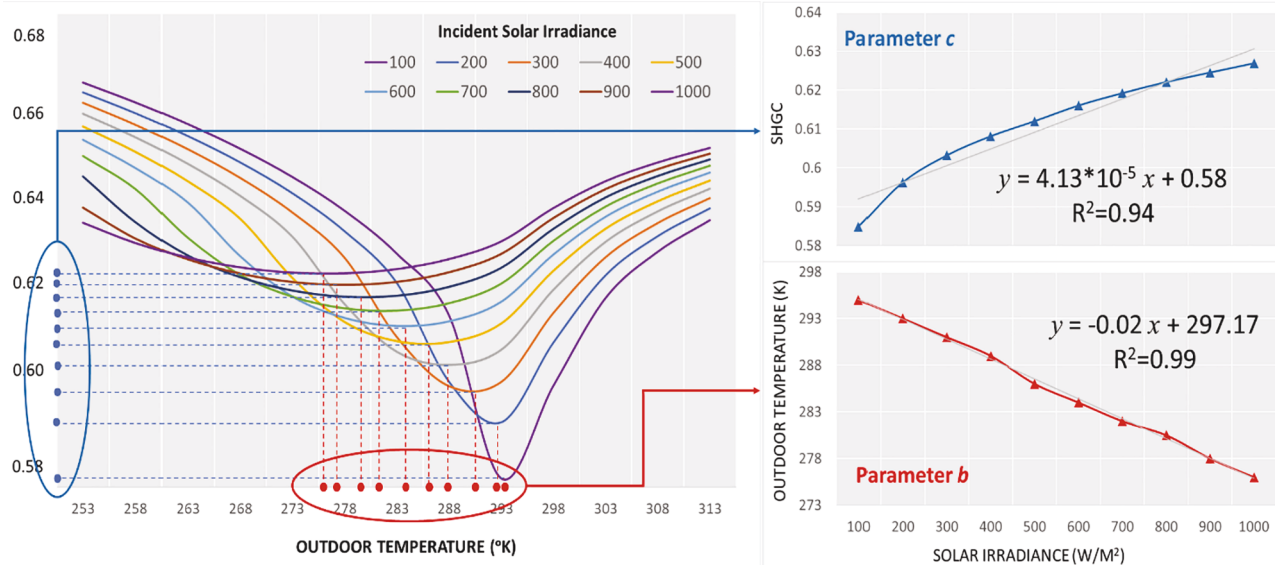

Fig. 9. Key parameters in the parabolic function of SHGC of the photothermal window.

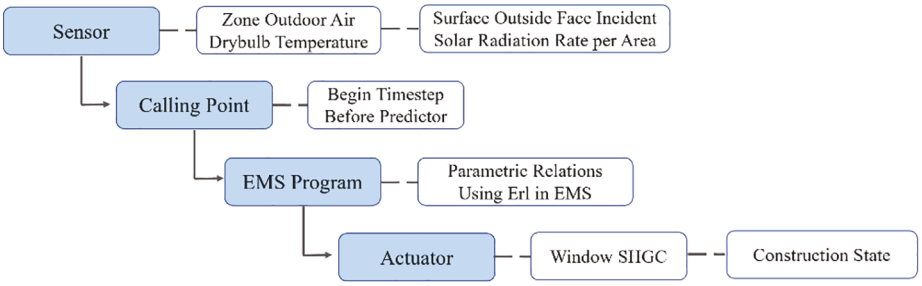

Fig. 10. EMS parametric energy simulation workflow.

understand the photothermal window's energy performance, three other window types were compared, including single-pane clear windows, single-pane low-e coated windows, and double-pane windows. The window properties used in this energy analysis are shown in Table 3.

The construction details of single-pane clear, single-pane Low-E, single-pane photothermal, and double-pane windows were set up in EnergyPlus and used to replace the original windows defined in the prototypical models. The settings in terms of other envelope components, such as roofs and walls, and building lighting and air conditioning system configurations were maintained the same in all models. This is to ensure that the performance comparison focuses on the window's impacts. The prototypical model consists of one core zone and four perimeter zones, one per cardinal direction. A series of whole-building annual energy simulations in different climates (Zones 3 to 6) was performed, and four cities, Atlanta (GA), Seattle (WA), Chicago (IL), and Great Falls (MT), were selected for each climate zone. Furthermore, we anticipated the potential overheating issues of the photothermal window application. So, to avoid the overheating issue in summer by the photothermal windows, we simply added overhangs to the photothermal window models. The overhang depth selection was upon the solar angles in the summer solstice of each representative city.

4. Result and discussion

4.1. Whole building's heating energy analysis

The energy use of a single-pane clear window was used as the baseline, and annual energy savings percentages for the single-pane Low-E, single-pane photothermal, and double-pane windows were calculated from the baseline. The annual heating loads and associated energy savings percentages for these four cities are reported in Fig. 11. It can be seen that the addition of a Low-E coating achieved 3.4% to 11.9% annual heating energy compared with the single-pane clear windows, which is mainly due to the increased thermal performance while some solar heat gain reductions relative to the single-pane clear windows occur because of Low-E coating. Comparatively, the photothermal windows led to greater heating energy savings in winter, ranging from 16.2% to 20.8% relative to the baseline model. In contrast to the single-pane Low-E windows, the photothermal window systems can further

Table 3
Window Properties Used in Whole Building Energy Analysis.

Window	U-factor(W/(m^2·K))	Solar Heat Gain Coefficient	Visible Transmittance	Emissivity
Single-pane clear	5.88	0.87	0.90	0.84 (surface 2)
Single-pane Low-E	3.28	0.55	0.76	0.05 (surface 2)
Single-pane photothermal	3.30	0.58–0.67	0.75	0.06 (surface 2)
Double-pane Low-E	2.42	0.53	0.68	0.05 (surface 3)

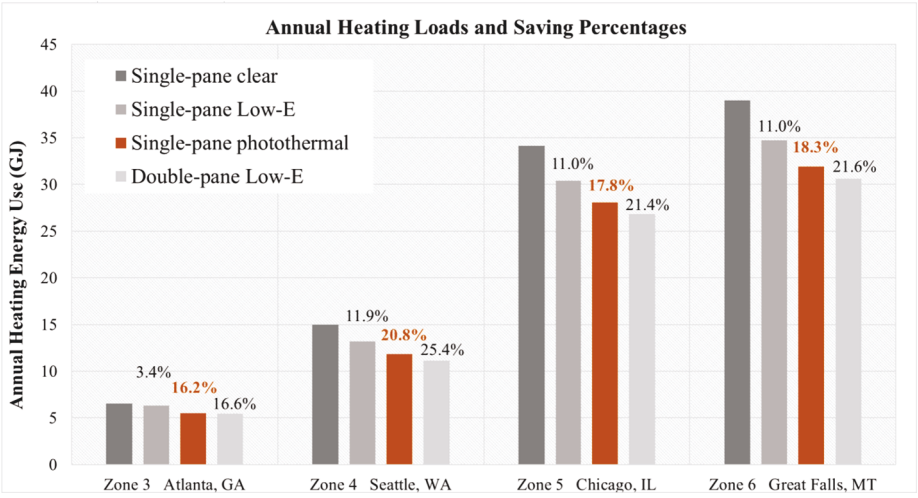

Fig. 11. Annual heating loads and associated savings percentages based on clear single-pane.

achieve 7.6–13.2% heating energy savings. Furthermore, we compared the energy performance of the designed photothermal windows to that of the double-pane windows. Regarding heating energy savings, the double-pane windows still outperformed the single-pane photothermal windows by averagely 3%, mainly due to the much lower U-factor of double-pane relative to single-pane windows (2.42 vs. 3.30).

4.2. Heat losses and gains through windows

It is worth mentioning that the above-mentioned heating energy saving percentages were calculated upon the whole building's scale, including the effects from all building envelope elements and systems, which might dilute the true impacts of the window performance improvements. When we only focus on the energy performance of window components, the comparison provides a more accurate assessment of using the photothermal window. Fig. 12 illustrates the solar heat gains

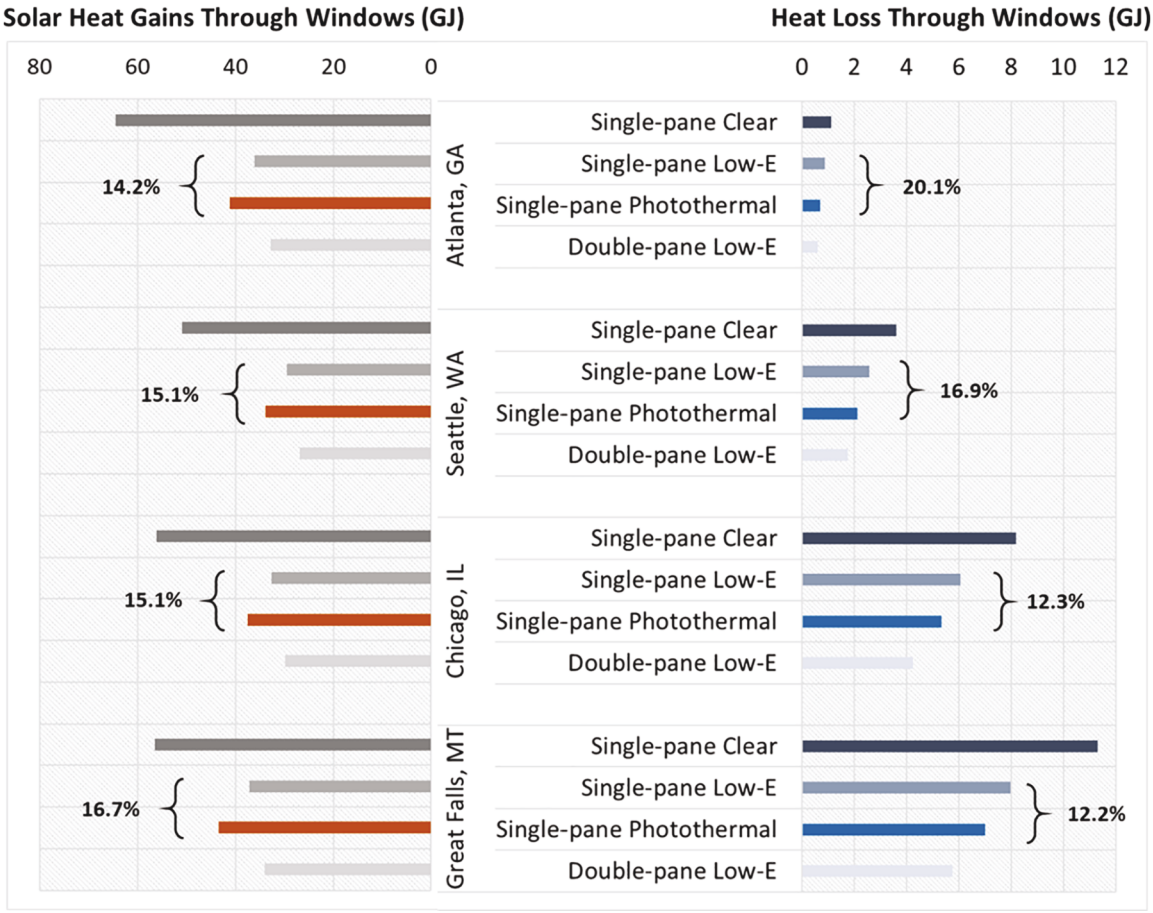

Fig. 12. Solar heat gains and building heat loss through windows.

and overall heat loss through window components in the different models. It demonstrates that the photothermal window can significantly reduce the heat loss, ranging from 34.9 to 40.8% depending on different climates, relative to the baseline window models. Compared with the Low-E window models, the photothermal windows also obviously outperformed, with about 12.2–20.1% heat loss reductions, as indicated in Fig. 12. The solar heat gain differences between them are also aligned with this observation. Although the transmitted solar radiations between the Low-E window and the photothermal window are almost the same, the PPE-enhanced inward-flowing heat of the photothermal windows enabled 14.2–16.7% more solar heat gains than that of the Low-E windows. The reduced heat loss and enhanced solar heat gains contributed to the resulting energy savings of the photothermal windows.

4.3. Discussion

Adhesive Low-E films are considered as one of the effective single-pane window retrofitting technologies, which could be installed as replacements for existing windowpanes without necessitating replacement of the sash in which the pane is mounted. Adding the nanoscale photothermal layer may further reduce the overall building heating energy use and window heat loss, which is mainly because of the nanoscale LSPR-driven PPE and the solar infrared energy utilization. In the conventional understanding, absorbing the solar radiation energy on the building windows, especially with the low-emissivity effect, is considered as the solar heat gain reduction strategy. Here we demonstrated a different perspective that was to enhance the solar heat gains. This conclusion is built upon two major facts: the strong NIR reflection by the Low-E coating and the presence of the interfacial insulation by the nanoscale PPE. These findings cast doubts on the conventional macroscopic heat transfer models and hypothesized a significant thermal barrier presence between the heating NPs and the substrate. Bearing this in mind, the photothermal procedure described and examined in this work is different from the conventional building materials' light-to-heat conversion but induced from the NPs, which led to a relatively larger fraction of inward-flowing heat converted from the solar infrared radiation.

Photothermal windows may increase summer cooling loads because of the possibility of overheating under solar radiation. However, with the overhang design in response to the high solar angles in summer, the incident solar irradiance may be dramatically reduced in summer but with no or small reduction in winter. Then, the decreased incident solar irradiance in the high outdoor temperature range may largely reduce $SHGC_{PPE}$, which can be explained by Eq. (10). As shown in Table 4, the simulation results show the annual cooling loads of the photothermal window models by using the overhang systems are only slightly higher than that of the single-pane Low-E window models of these four cities, which demonstrates the effectiveness of the overhang systems to control the overheating issues when using the photothermal window. Although the addition of overhangs would somehow reduce the heating energy, the annual energy saving would be still expected. There is a trade-off between the heating energy decrease and the cooling energy increase when it comes to the nanoscale PPE, so the optimal overhang depth and the nanoscale PPE intensity would exist. However, the optimization potion was not included in this research scope and could be explored in the future.

Table 4
Cooling energy use comparison between Low-E and photothermal windows.

Zone	City	Single-pane Low-E (GJ)	Singe-pane photothermal w/o overhangs (GJ)	Singe-pane photothermal w overhangs (GJ)
3	Atlanta, GA	77.1	84.9	77.9
4	Seattle, WA	40.5	45.9	41.4
5	Chicago, IL	52.5	58.1	53.4
6	Great Falls, MT	43.2	49.5	43.5

Also, the surface plasmon mode has a hybrid nature – propagating surface plasmon polaritons and localized surface plasmons, providing additional pathways for harvesting the energy of below-gap photons (e.g., below the semiconductor bandgap) to generate photocurrent with metal–insulator-metal structure design [10,11,12]. So, it is possible to design specific multilayer structures and some electronic wiring to exhibit switchable photothermal and photoelectrical features, achieving the seasonal dependent dynamic NIR modulation. In the meantime, other studies have identified the angular features of nanoscale PPE, which indicates much stronger temperature increases under smaller incident angles (e.g., low solar positions in winter) relative to the greater incident angles (e.g., high solar positions in summer) [37,49]. The research team will incorporate a previous study of seasonal solar NIR modeling into this angular-dependent model and examine the potential energy performance [50].

Furthermore, it is no doubt that the thermal performance of double-pane windows leads to more energy savings for both summer and winter relative to the photothermal windows. However, the use of double-pane windows slightly reduced the VT, so the interior lighting energy use could be relatively higher than that when the single-pane photothermal window is used. Considering both the heating and lighting energy results, the photothermal single-pane windows might have very similar energy performances in relation to the performance of the double-pane windows. Also, as mentioned in the introduction, upgrading a single-pane window to a double-pane window in an existing building requires replacing the entire window, including frame, sash, glazing, and possibly the wall structure, due to the weight being doubled. Therefore, theretrofitting technology that can be used with existing single-pane window systems has long been sought after. Developing and adding the adhesive photothermal film may be an effective retrofitting solution for the single-pane window sector. In addition, as for new buildings, considering the relatively simpler installation, lighter weight, and lower cost, the single-pane photothermal window may still be preferable from the economical perspective. To make accurate decisions, some comprehensive cost-benefit analyses, taking different weather conditions, building typologies, durability, and maintenance into account, should be performed.

Last, in winter, the temperature of the single-pane window's inner surface could be nearly as low as the outdoor temperature. The consequence is that the near-window zone will be uncomfortably chilly compared to the rest of the heated interior. Also, the cold temperature of the windowpane will have high condensation risks, which may be degraded by applying the inner Low-E coating. This is possibly addressed by using the photothermal fim as well. The window's inner surface will be warm upon solar radiation because of the presence of the photothermal materials, which may not only mitigate the programs of Low-E coated single-panes with comfort but also enhance the condensation resistance.

5. Conclusion

This research examined the energy savings potential of surface plasmon-induced NP photothermal effects used on single-pane windows, which are believed to address one of the major retrofit-related issues in the building energy sector. Previous studies have shown the possible effects of using photothermal films to coat windows on building energy; however, a comprehensive energy analysis had never been conducted.

To resolve this gap, a simplified analytical model incorporated with interfacial insulation that addresses the surface localized heating on one surface of the glass pane was developed and validated via photothermal

experiments in the lab. This model can be used to compute the temperature profiles of photothermal windows under various design conditions and boundaries. Subsequently, the validated analytical model was used to analyze the improved thermal performance relative to the Low-E single-panes. In particular, the dynamic SHGC (i.e., $SHGC_{PPE}$ in this work) features were characterized and a physics-based mathematical model was obtained based on a series of numerical analyses and representative boundary combinations (outdoor temperature and solar irradiance). Last, to understand the overall energy performance of the photothermal windows, we employed a parametric energy simulation method to take the temperature- and solar irradiance- dependent SHGC into account. The results show the photothermal coating can be used as a new energy-efficient retrofit technology for single-pane windows, with an energy saving potential **16.2–20.8%.** Compared to the Low-E technology, 12.2–20.1% heat loss reduction and 14.2–16.7% more solar heat gains through the windows and **7.6–13.2%** energy savings on the whole building's heating energy scale can be still obtained by using the photothermal windows, which appear very close to the thermal performance of the double-pane windows in winter seasons under conventional solar radiation. Most importantly, these research findings open up a wide range of innovative solar energy utilization in building window systems. When considering potential condensation effects and local discomfort driven by the Low-E coated single-panes, the photothermal windows may achieve more benefits. The photothermal windows also showed very similar energy-saving performance relative to the double-pane windows, especially when the lighting energy use was also considered in this comparison. Notably, the energy savings were not achieved by increasing the thermal insulation through the additional air layer or the insulating materials, but rather by the NP's surface plasmon-induced photothermal effect and utilization of solar NIR energy. This was also achieved without compensating for VT.

Credit authorship contribution statement

Enhe Zhang: Investigation and Numerical Analysis. **Qiuhua Duan:** Modeling and Simulation. **Julian Wang:** Conceptualization, Methodology, Project administration. **Yuan Zhao:** Material Synthesis and Experiments. **Yanxiao Feng:** Data Modeling and Visualization.

Declaration of Competing Interest

The authors declare that they have no known competing financial interests or personal relationships that could have appeared to influence the work reported in this paper.

Acknowledgement

We acknowledge the financial support provided by the National Science Foundation CMMI-2001207 and National Science Foundation CMMI-1953004, and USDA Natural Resources Conservation Service NR203A750008G006.

References

[1] Peng J, Curcija DC, Thanachareonkit A, Lee ES, Goudey H, Selkowitz SE. Study on the overall energy performance of a novel c-Si based semitransparent solar photovoltaic window. Appl Energy 2019;242:854–72. https://doi.org/10.1016/j.apenergy.2019.03.107.
[2] EIA. Residential Energy Consumption Survey (RECS) – Data; 2015.
[3] Advanced Research Projects Agency – Energy (Arpa-E) Single-Pane Highly Insulating Efficient Lucid Designs; 2015.
[4] Rissman J. Low-Emissivity Windows. Am Energy Innov Counc 2013;12.
[5] Wang J, Shi D. Spectral selective and photothermal nano structured thin films for energy efficient windows. Appl Energy 2017;208:83–96. https://doi.org/10.1016/j.apenergy.2017.10.066.
[6] Schiff E. Single-pane window efficiency. ARPA-E Work; 2014.
[7] Song Y, Duan Q, Feng Y, Zhang E, Wang J, Niu S. Solar Infrared Radiation towards Building Energy Efficiency: Measurement, Data, and Modeling. Environ Rev 2020.
[8] Ji J, Zhou S, Wang W, Ling F, Yao J. Active control of terahertz plasmon-induced transparency in the hybrid metamaterial/monolayer MoS2/Si structure. Nanoscale 2019;11(19):9429–35. https://doi.org/10.1039/C8NR08813F.
[9] Le Perchec J, Desieres Y, Rochat N, Espiau de Lamaestre R. Subwavelength optical absorber with an integrated photon sorter. Appl Phys Lett 2012;100(11):113305. https://doi.org/10.1063/1.3694749.
[10] Wang F, Melosh NA. Plasmonic energy collection through hot carrier extraction. Nano Lett 2011;11(12):5426–30. https://doi.org/10.1021/nl203196z.
[11] Chalabi H, Brongersma ML. Plasmonics: Harvest season for hot electrons. Nat Nanotechnol 2013;8(4):229–30. https://doi.org/10.1038/nnano.2013.49.
[12] Shinde SL, Ngo HD, Ngo TD, Ishii S, Nagao T. Solar-active titanium-based oxide photocatalysts loaded on TiN array absorbers for enhanced broadband photocurrent generation. J Appl Phys 2021;129(2):023103. https://doi.org/10.1063/5.0031400.
[13] Xu Q, Liu X, Xuan Y, Xu Y, Liu D. High-performance infrared thermal radiation suppression metamaterials enabling inhibited infrared emittance and decreased temperature simultaneously. Int. J Heat Mass Transf 2020;161:120318. https://doi.org/10.1016/j.ijheatmasstransfer.2020.120318.
[14] Feng R, Qiu J, Liu L, Ding W, Chen L. Parallel LC circuit model for multi-band absorption and preliminary design of radiative cooling. Opt Express 2014;22(S7):A1713. https://doi.org/10.1364/OE.22.0A1713.
[15] Zhao B, Chen K, Buddhiraju S, Bhatt G, Lipson M, Fan S. High-performance near-field thermophotovoltaics for waste heat recovery. Nano Energy 2017;41:344–50. https://doi.org/10.1016/j.nanoen.2017.09.054.
[16] Papadakis GT, Buddhiraju S, Zhao Z, Zhao B, Fan S. Broadening Near-Field Emission for Performance Enhancement in Thermophotovoltaics. Nano Lett 2020;20(3):1654–61. https://doi.org/10.1021/acs.nanolett.9b04762.
[17] Chen W, Ouyang J, Liu H, Chen M, Zeng K, Sheng J, et al. Black Phosphorus Nanosheet-Based Drug Delivery System for Synergistic Photodynamic/Photothermal/Chemotherapy of Cancer. Adv Mater 2017;29(5):1603864. https://doi.org/10.1002/adma.201603864.
[18] Kim M, Lee J, Nam J. Plasmonic Photothermal Nanoparticles for Biomedical Applications. Adv Sci 2019;6(17):1900471. https://doi.org/10.1002/advs.v6.1710.1002/advs.201900471.
[19] Li Z, Liu J, Hu Y, Howard KA, Li Z, Fan X, et al. Multimodal Imaging-Guided Antitumor Photothermal Therapy and Drug Delivery Using Bismuth Selenide Spherical Sponge. ACS Nano 2016;10(10):9646–58. https://doi.org/10.1021/acsnano.6b0542710.1021/acsnano.6b05427.s001.
[20] Liu G, Xu J, Wang K. Solar water evaporation by black photothermal sheets. Nano Energy 2017;41:269–84. https://doi.org/10.1016/j.nanoen.2017.09.005.
[21] Link S, El-Sayed MA. Shape and size dependence of radiative, non-radiative and photothermal properties of gold nanocrystals. Int Rev Phys Chem 2000;19(3):409–53. https://doi.org/10.1080/01442350050034180.
[22] Boriskina SV, Ghasemi H, Chen G. Plasmonic materials for energy: From physics to applications. Mater Today 2013;16(10):375–86. https://doi.org/10.1016/j.mattod.2013.09.003.
[23] Neumann O, Urban AS, Day J, Lal S, Nordlander P, Halas NJ. Solar vapor generation enabled by nanoparticles. ACS Nano 2013;7(1):42–9. https://doi.org/10.1021/nn304948h.
[24] Xu Y, Zhao X, Li A, Yue Y, Jiang J, Zhang X. Plasmonic heating induced by Au nanoparticles for quasi-ballistic thermal transport in multi-walled carbon nanotubes. Nanoscale 2019;11(16):7572–81. https://doi.org/10.1039/C9NR00901A.
[25] Oyake T, Sakata M, Shiomi J. Nanoscale thermal conductivity spectroscopy by using gold nano-islands heat absorbers. Appl Phys Lett 2015;106(7):073102. https://doi.org/10.1063/1.4913311.
[26] Chen G. Nonlocal and nonequilibrium heat conduction in the vicinity of nanoparticles. J Heat Transfer 1996;118. Doi: 10.1115/1.2822665.
[27] Adleman JR, Boyd DA, Goodwin DG, Psaltis D. Heterogenous catalysis mediated by plasmon heating. Nano Lett 2009;9(12):4417–23. https://doi.org/10.1021/nl902711n.
[28] Atanasov PA, Nedyalkov N, Imamova SE, Miyanishi T, Obara M. Substrate nanomodification based on heating and near field properties of gold nanoparticles. Int J Nanoparticles 2010;3(3):206. https://doi.org/10.1504/IJNP.2010.035876.
[29] Fang Z, Zhen Y-R, Neumann O, Polman A, García de Abajo FJ, Nordlander P, et al. Evolution of light-induced vapor generation at a liquid-immersed metallic nanoparticle. Nano Lett 2013;13(4):1736–42. https://doi.org/10.1021/nl4003238.
[30] Carlson MT, Green AJ, Richardson HH. Superheating water by CW excitation of gold nanodots. Nano Lett 2012;12(3):1534–7. https://doi.org/10.1021/nl2043503.
[31] Abarbanel D, Maassen J. Modeling quasi-ballistic transient thermal transport with spatially sinusoidal heating: A McKelvey-Shockley flux approach. J Appl Phys 2017;121(20):204305. https://doi.org/10.1063/1.4984202.
[32] Li Y, Liu J, Liang J, Yu X, Li D. Tunable solar-heat shielding property of transparent films based on mesoporous Sb-doped SnO2 microspheres. ACS Appl Mater Interfaces 2015;7(12):6574–83. https://doi.org/10.1021/am508711p.
[33] V. Besteiro L, Kong X-T, Wang Z, Rosei F, Govorov AO. Plasmonic Glasses and Films Based on Alternative Inexpensive Materials for Blocking Infrared Radiation. Nano Lett 2018;18(5):3147–56. https://doi.org/10.1021/acs.nanolett.8b0076410.1021/acs.nanolett.8b00764.s001.
[34] Shen B, Wang Y, Lu L, Yang H. Synthesis and characterization of Sb-doped SnO2 with high near-infrared shielding property for energy-efficient windows by a facile dual-titration co-precipitation method. Ceram Int 2020;46(11):18518–25. https://doi.org/10.1016/j.ceramint.2020.04.157.

[35] Zhao Y, Sadat ME, Dunn A, Xu H, Chen C-H, Nakasuga W, et al. Photothermal effect on Fe3O4 nanoparticles irradiated by white-light for energy-efficient window applications. Sol Energy Mater Sol Cells 2017;161:247–54. https://doi.org/10.1016/j.solmat.2016.11.039.
[36] Guo M, Gao L, Wei Y, Ma Y, Jianyong Y, Ding B. Solar transparent radiators based on in-plane worm-like assemblies of metal nanoparticles. Sol Energy Mater Sol Cells 2021;219:110796. https://doi.org/10.1016/j.solmat.2020.110796.
[37] Lyu M, Lin J, Krupczak J, Shi D. Light angle dependence of photothermal properties in oxide and porphyrin thin films for energy-efficient window applications. MRS Commun 2020;10(3):439–48. https://doi.org/10.1557/mrc.2020.39.
[38] Lin J, Zhao Y, Shi D. Optical thermal insulation via the photothermal effects of Fe3O4 and Fe3O4@Cu2-xS thin films for energy-efficient single-pane windows. MRS Commun 2020;10(1):155–63. https://doi.org/10.1557/mrc.2020.4.
[39] Tian Q, Hu J, Zhu Y, Zou R, Chen Z, Yang S, et al. Sub-10 nm Fe3O4@Cu2-xS core-shell nanoparticles for dual-modal imaging and photothermal therapy. J Am Chem Soc 2013;135(23):8571–7. https://doi.org/10.1021/ja4013497.
[40] ISO15099. ISO15099:2003 Thermal performance of windows, doors and shading devices - detailed calculations. Indian Ceram 2003.
[41] Curcija DC, Zhu L, Czarnecki S, Mitchell RD, Kohler C, Simon V. Vidanovic CH. BERKELEY LAB WINDOW; 2015.
[42] Chen F, Wittkopf SK, Khai Ng P, Du H. Solar heat gain coefficient measurement of semi-transparent photovoltaic modules with indoor calorimetric hot box and solar simulator. Energy Build 2012;53:74–84. https://doi.org/10.1016/j.enbuild.2012.06.005.
[43] Wang C, Shi Y, Yang D-R, Xia X-H. Combining plasmonics and electrochemistry at the nanoscale. Curr Opin. Electrochem 2018;7:95–102. https://doi.org/10.1016/j.coelec.2017.11.001.
[44] Wang X, Sridhar V, Guo S, Talebi N, Miguel-López A, Hahn K, et al. Fuel-Free Nanocap-Like Motors Actuated Under Visible Light. Adv Funct Mater 2018;28. Doi: 10.1002/adfm.201705862.
[45] Liu Z, Huang Y, Xiao Q, Zhu H. Selective reduction of nitroaromatics to azoxy compounds on supported Ag-Cu alloy nanoparticles through visible light irradiation. Green Chem 2016;18(3):817–25. https://doi.org/10.1039/C5GC01726B.
[46] NATIONAL FENESTRATION RATING COUNCIL. Procedure for Interim Standard Test Method for Measuring the Solar Heat Gain Coefficient of Fenestration Systems Using Calorimetry Hot Box Methods,NFRC 201-2017; 2013.
[47] Wang JJ, Beltran L. A method of energy simulation for dynamic building envelopes. Proc. SimBuild 2016:1.
[48] Wang JJ, Beltran L. Energy Performance of Future Dynamic Building Envelopes. Proc. 3rd Ibpsa- Conf. BSO 2016.
[49] Taylor AB, Chon JWM. Angular Photothermal Depletion of Randomly Oriented Gold Nanorods for Polarization-Controlled Multilayered Optical Storage. Adv Opt Mater 2015. https://doi.org/10.1002/adom.201400294.
[50] Duan Q, Zhao Y, Wang J. Thermal performance and condensation risk of single-pane glazing with low emissivity coatings. MRS Adv 2020:1–10.